Immunofluorescence of Intracellular Targets in Live Cells

Alexandra Koriath

A thesis

submitted in partial fulfillment of the

requirements for the degree of:

Master of Science in Bioengineering

University of Washington

2022

Committee:

Xiaohu Gao

Andre Berndt

Program Authorized to Offer Degree:

Bioengineering

University of Washington

Abstract

Immunofluorescence of Intracellular Targets in Live Cells

Alexandra Koriath

Chair of the Supervisory Committee:

Xiaohu Gao

Department of Bioengineering

Every second, living human cells are executing complex functions to initiate or influence various processes such as energy production, growth, metabolism and reproduction. This also means that intracellular structures are rapidly moving and morphing as the various proteins and organelles interact. Two important goals for scientists attempting to understand and manipulate intracellular processes are to visualize structural movements within the cell and to use specifically generated proteins to adjust interactions within the cell. Both aims could be achieved if the desired proteins were able to cross through the cell membrane lipid bilayer. Currently, the methods for delivering proteins into live cells can compromise the integrity of the cell's defenses, are very inefficient to use or they rely on endocytosis, a natural process that ends in the degradation of many proteins. Recently, members of the University of Washington's Gao Lab have made a breakthrough by creating a cholesterol tag that aids in delivery of proteins across the cell membrane. In this study, a second-generation hydrophobic tag was tested for functionality in delivery of single domain

antibodies, Fab fragments, and full-sized antibodies into live cells. Better understanding the functions and limits of this cytosolic-delivery method will increase the accessibility of live-cell fluorescent imaging and open new possibilities in the field of intracellular protein therapies.

INTRODUCTION:

Since the sequencing of the human genome, scientists have been able to generate accurate lists of druggable human genes [1]. Along with these lists has come the identification of various so called “undruggable” targets that, due to their locations and protein-protein interaction (PPI) interfaces, cannot yet be drugged using traditional methods [2]. One class of these targets, the family of Ras proteins, has mutated forms that are involved in many forms of cancer [3]. Another “undruggable” target class includes various proteins in the ubiquitin system, a post-translational process that leads to protein degradation, dysregulation of which is involved in cancer and neurodegenerative diseases [4]. Finding ways to reach and affect these targets, and others relating to metabolic diseases and genetic disorders, would have a huge impact on medicine and lower the burden that these conditions put on large parts of the population.

The two classes of clinically approved drugs that are traditionally used are small molecule drugs and biologics [5]. Small molecule drugs can easily enter the cell membrane and affect intracellular targets, but they are unable to bind to the PPI interfaces of “undruggable” targets. Biologics, such as antibodies, have large surface areas and can interact with these PPI interfaces, but their large size makes travelling past the cell membrane difficult [6]. Currently, antibodies are approved for therapeutic use on extracellular targets, but there are no approved clinical methods for use of antibodies against intracellular targets [7]. Developing a method for intracellular delivery of antibodies that is efficient and minimally cytotoxic, could allow for drugging of various targets that were previously labeled as undruggable.

Another application for functional delivery of target-binding proteins into live cells is imaging. Imaging is important in helping scientists better understand movement and interactions within the cell and can also be used for drug screening [8], [9]. The wide range of targets that can be bound by antibodies, as well as their specificity means they are a good option for fluorescent imaging, but they are currently primarily used in fixed cells in immunocytochemistry or against extracellular targets [10]–[12]. Having the ability to easily deliver fluorescent-labeled antibodies within the cell would open many options for live cell imaging.

Currently, the methods for delivering proteins, such as antibodies, into live cells are problematic because they can compromise the integrity of the cell's defenses, are very inefficient to use or can lead to intracellular delivery via endocytosis [13]. Endocytosis is a built-in cell mechanism that allows extracellular particles to enter the cell; however, if the particles that enter through this process are not recognized by the cell, they will be degraded [14]. This degradation means that not only are you losing a high volume of the protein you hope to deliver, but that many fluorophores are stuck in endosomes creating a high level of background in the cell if imaging attempts are made.

The two most prominent physical methods for intracellular delivery are microinjection and electroporation, but both methods have issues. The drawback for microinjection is that it can only be performed on a few cells at once which leads to low experimental throughput [15]. Electroporation can damage the integrity of the cell wall, often causing cytotoxicity and affecting cell functions [16]. Both methods also require physical access to the cell to be functional.

Another promising method for intracellular therapies involves expression of antibodies inside the cell, using plasmids and intracellular antibody (intrabody) sequences [6]. While this method has potential for therapy applications, there is minimal research on the effect that altering cellular expression can have on cell function. Expression of other proteins, such as green fluorescent protein, are also used for various imaging applications, but, again, this requires spending time to manipulate cellular expression which may also cause unwanted interactions in the cell [8], [9].

The final and most broad field of study involving intracellular protein delivery is that of nanocarriers. This process involves a small organic or inorganic carrier bringing the desired protein into the cell as cargo [6]. These methods are the most likely to lead to endocytosis-related issues during delivery and have varying levels of cytotoxicity. Nanocarriers fall into multiple categories including lipid-based, polymer-based, viral, viral-like and inorganic. Recent tests in liposome-based delivery have shown successful delivery of antibodies as well interactions between these antibodies and intracellular targets [17]. Polymer studies have also shown promise, with interactions occurring between delivered biomacromolecules and cellular functions and leading to induction of apoptosis in cancer cells [18].

The delivery method being probed in this study falls under the category of nanocarrier delivery. The “nanocarriers” are hydrophobic tags consisting of a Coomassie Blue molecule (CB) with two alkyl tails (Figure 1). For the delivery process, multiple tags are bound to a protein via the CB molecule, leaving the hydrophobic tags facing the solution that the protein is in and creating a hydrophobic shell around the protein (Figure 2). When incubated with cells, it is favorable for the hydrophobic protein complex to move within the hydrophobic cell membrane lipid bilayer.

Overtime, the tags will begin to dissociate from the protein, exposing its hydrophilic surface. The hydrophobic lipid bilayer is then no longer a favorable location for the hydrophilic protein, so it will slip out into the cytosol. Because this delivery process avoids endocytosis, there is no degradation of delivered proteins and extra background fluorescence in imaging can be avoided.

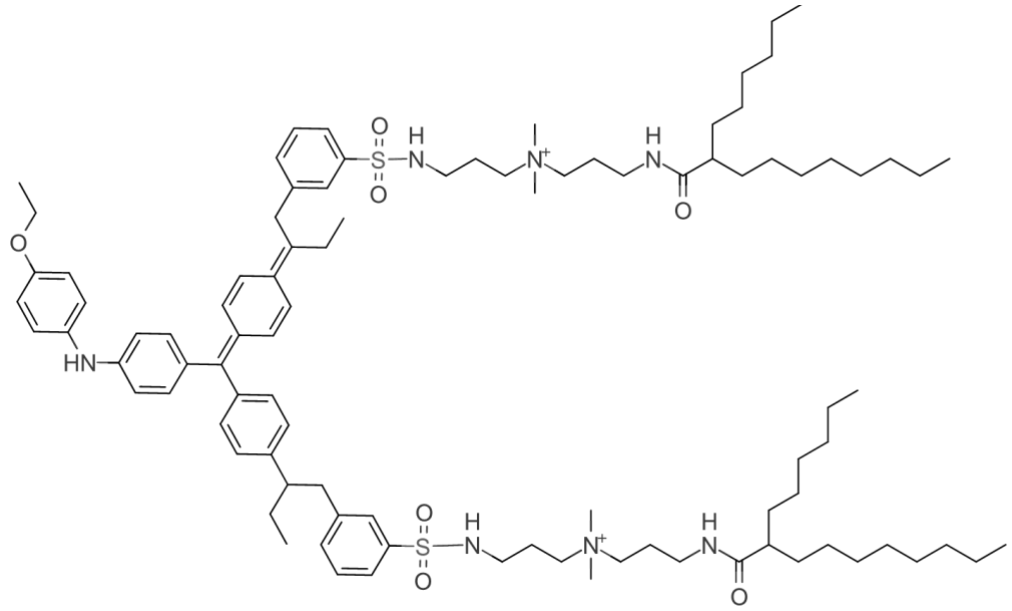

Figure 1: *Schematic diagram of the synthesized second-generation CB-alkyl tag.*

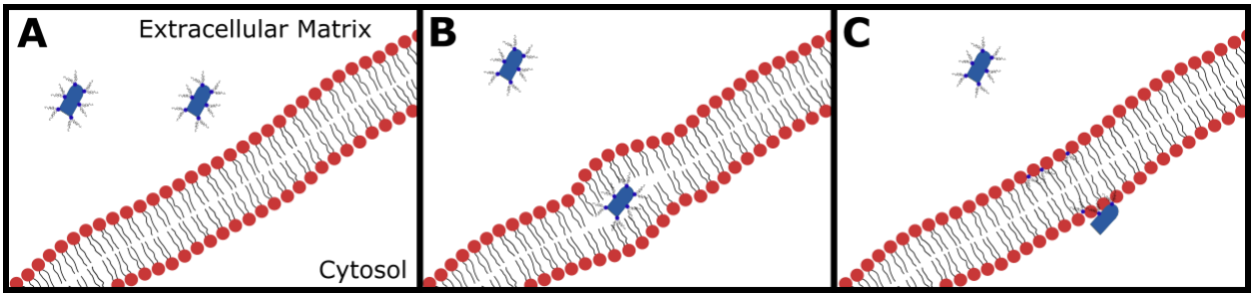

Figure 2: *(A) Tagged proteins have Coomassie blue G250 molecules anchored to their surface leaving the cholesterol "tails" facing outward to provide compatibility with the cell membrane lipid bilayer. (B) This allows proteins to become temporarily imbedded in the bilayer. (C) After a time, each tagged protein will dissociate from the tags and their hydrophilic nature will cause them to be ejected from the membrane and into the cytosol.*

Initial testing of this delivery method, using a first generation CB tag with cholesterol tails, showed various levels of success in delivery of proteins with sizes ranging from 6.5-150 kDa [19]. Delivery efficiency was shown to increase the smaller the size of the protein. In the previous study, there were no tests done on cytotoxicity of the delivery method or tag, so this is an important aspect that was focused on in this study.

Full-sized antibodies with a large molecular weight of 150 kDa are often less compatible with many methods of intracellular delivery, but there are multiple antibody-derived immunological agents that maintain the functionality of antibodies at a much smaller size (Figure 3) [20]. F(ab') fragments and F(ab')2 fragments can be easily created in most labs by using predeveloped kits to digest full sized antibodies. More recently, single domain antibodies (sdAbs), also known as VHH antibodies or nanobodies, have become more commonly used [21]. These much smaller proteins are derived from heavy chain only antibodies that are found in camelid species, such as llamas. While the small size of these immunological agents makes them more versatile, the variety of targets for which they are available is minimal and synthesis is time consuming and expensive. Full-sized antibodies, and therefore F(ab') and F(ab')2 fragments, are available for almost any target, so if these larger proteins can be delivered into cells, that would be much more useful given the current state of immunological agent availability.

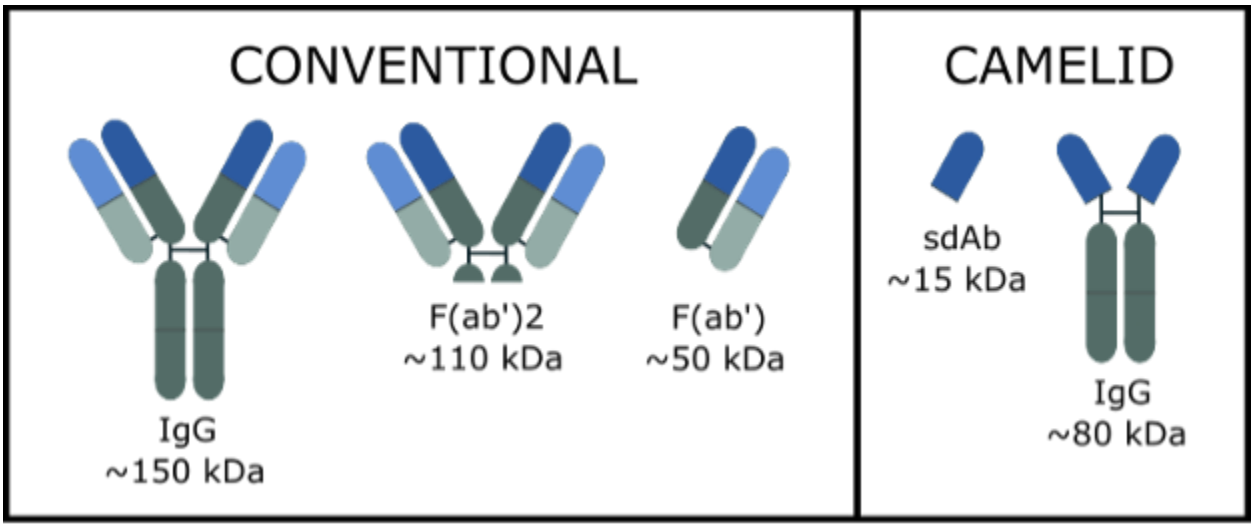

Figure 3: *Conventional antibodies, often derived from humans or mice, have a relatively large molecular weight. Fragments of the binding region of these proteins, F(ab')2 and F(ab'), maintain the binding functionality of the protein at a smaller size. Camelid antibodies, generally derived from llamas, feature a smaller binding domain than conventional antibodies. A single domain antibody (sdAb) can be generated from the camelid antibody that maintains binding ability at a molecular weight even smaller than F(ab')2 and F(ab').*

In this study, sdAbs, Fab fragments and various antibodies were prepared for delivery using the alkyl-CB tag delivery method. In some cases, the protein:tag ratio was varied to increase delivery success. The results of delivery for each of the cargos were determined using brightfield and fluorescent imaging. Cytotoxicity of the delivery method was visualized both through fluorescent cell stains as well as visualization of cell shape.

MATERIALS AND METHODS:

General:

Unless otherwise noted, all organic solvents and chemicals were purchased from Sigma-Aldrich. Histone-Label was purchased from Proteintech. Pierce™ Mouse IgG1 Fab and F(ab')2 Micro Preparation Kit, NuPAGE™ 12%, Bis-Tris, 1.0 mm, Mini Protein Gels, NuPAGE MOPS SDS Running Buffer, NuPAGE LDS Sample Buffer, PageRuler™ Plus Prestained Protein Ladder (10

to 250 kDa), LIVE/DEAD™ Viability/Cytotoxicity Kit, Zeba™ Spin Desalting Columns, 7K MWCO, 0.5 mL, Pierce™ Antibody Clean-up Kit, Alexa Fluor™ 488 NHS Ester (Succinimidyl Ester), Mouse anti-Human IgG1 Fc Secondary Antibody (Alexa Fluor™ 488), GAPDH Loading Control Monoclonal Antibody (GA1R), and HDAC1 Monoclonal Antibody (4C4G7), CoraLite®594 were purchased from ThermoFisher Scientific. Alexa Fluor® 488 anti-Vimentin Antibody was purchased form BioLegend. Image analysis was completed using the National Institute of Health program, ImageJ.

Cell Culture:

HeLa (ATCC #CCL-2) cell lines were obtained from the American Type Culture Collection (ATCC). The cells were cultured on 35 mm polystyrene plates in Eagle's minimal essential medium supplemented with FBS (10%), penicillin (100 U/ml), and streptomycin (100 μg/ml) and propagated in a humidified 5% CO_2 incubator at 37°C. Glass-bottom dishes (Cellvis) coated in poly-d-lysine (Gibco) according to manufacturer's instructions were used for all imaging experiments.

Protein Preparation:

The Pierce™ Mouse IgG1 Fab and F(ab')2 Micro Preparation Kit was used according to protocol for digestion of Mouse anti-Human IgG1 Fc Secondary Antibody (Alexa Fluor™ 488) into Fab fragments. The resulting solution was desalted with buffer exchange to PBS and stored at 4°C. Digestion completion and protein purification were confirmed through protein electrophoresis.

The Pierce™ Antibody Clean-up Kit was used according to protocol to remove BSA from the unconjugated antibody, GA1R. The resulting GA1R solution underwent buffer exchange to a borate buffer, pH 8.5. Alexa Fluor™ 488 NHS Ester was added to the GA1R solution at an antibody:dye ratio of 1:20 and incubated at room temperature overnight. The solution was desalted with buffer exchange to PBS and stored at 4°C.

Protein Tagging:

Purified CB-alkyl tag powder was synthesized using a modified version of the one described in the Tai et. al 2020 publication (Appendix A), reconstituted with ethanol/water (4:1, v/v) to a concentration of 1.6 mM and stored at -20°C as a stock. Before tagging, the concentration of each protein solution was diluted to 25 μM. Volumes of protein and hydrophobic-CB tag calculated according to the desired protein to tag ratio were added to an Eppendorf microcentrifuge tube and mixed by pipetting. The mixture was incubated in a water bath at 37°C for 8 minutes before being removed and sonicated in an ultrasonic water bath for at least 30 seconds. The mixture was again incubated in a water bath at 37°C for 8 minutes.

Cellular Delivery:

In all sdAb testing, the protein concentration and protein:tag ratio were varied, while the final tag concentration was maintained at 2 μM. For testing with Fab fragments and antibodies, the protein concentration and protein:tag ratio were varied, while the final tag concentration was maintained at 1 μM. Due to variability in purchased antibody concentration the antibody delivery protein:tag ratios ranged from about 1:8 to 1:25 for best results. The previously published ratio for antibody delivery was 1:16 [19].

Cells were seeded in a 24-well plate in supplemented Eagle's minimum essential medium (Invitrogen) 1 day before the experiments. For protein delivery, the supplemented media was removed, and the cell monolayer was washed once with serum-free MEM. A solution of serum-free MEM containing the tagged protein at varying concentrations was added to each well and cells were incubated at 37°C for two hours. After treating, the serum-free tag-containing media was removed and replaced with supplemented media. Cells were then incubated at 37°C for one hour. For imaging, the supplemented media was removed and replaced with PBS to minimize background fluorescence. To test cell death in treated wells, cells were incubated at room temperature for 30 minutes in a PBS solution of 4 μM EthD-1 (EB) and then imaged. All media additions and washes were performed with wide-bore or cut pipet tips.

Microscopy:

An Olympus IX-71 inverted fluorescence microscope (Center Valley, PA) equipped with a true-color charge-coupled device (QColor5, Olympus) and a HSI camera (Nuance, 420–720 nm spectral range, CRI, now Advanced Molecular Vision) was primarily used for cell imaging. Images were obtained with a 10X dry objective and a 40X oil-immersion objective (Olympus). A wide UV filter cube (330–385 nm band-pass excitation, 420 nm long-pass emission, Olympus) and a mercury lamp light source combined with Rhodamine LP set cube (band-pass excitation 530-560 nm, long-pass emission 572 nm, Chroma, Bellows Falls, VT) were used for fluorescence imaging. Confocal images were taken using a Zeiss 710 LSM Confocal, Zeiss Axio Observer Z.1 microscope and 20X dry objective.

RESULTS AND DISCUSSION:

Single Domain Antibodies:

An sdAb against the intracellular target, histone H2A-H2B heterodimer, was chosen for initial testing of the delivery method. The sdAb, Histone-Label, has a molecular weight of about 15 kDa and is labeled with ATTO488. The Histone-Label was chosen due to the concentrated location of the targets in the cells' nuclei, which allowed for better visualization of delivery.

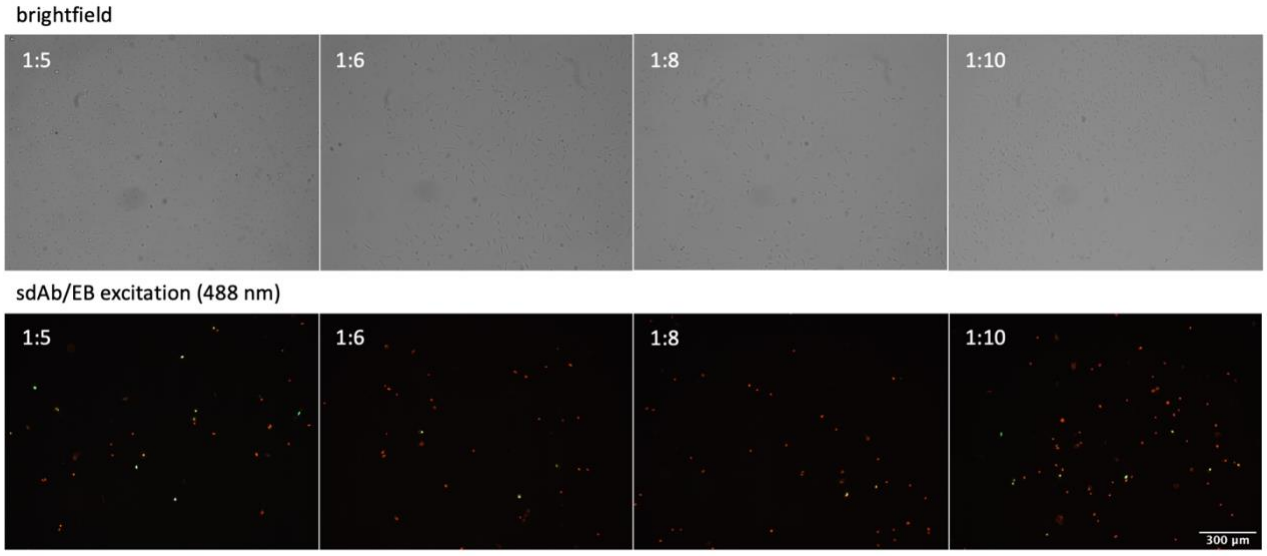

Figure 4: *Histone-Label delivered using protein:tag ratios of 1:5, 1:6, 1:8 and 1:10. Each condition used a final tag concentration of 2 µM. Dead cells were stained with EB according to protocol.*

Based on protein:tag ratios used on similarly sized proteins in the Tai et. al 2020 publication, the Histone-Label was prepared for delivery using ratios 1:5, 1:6, 1:8 and 1:10 (Figure 4). All these conditions showed nonuniform delivery, with a few cells showing brightly fluorescing nuclei and others with no fluorescence. Upon dead cell staining it was seen that many of the cells with bright nuclei, as well as others that did not show visual signs of delivery, were dead. One explanation for the cell death could be an excess of free-floating tags in the solution that are embedding in and disturbing the structural stability of the cell membrane. The cholesterol-CB tag and, therefore, the alkyl-CB tag was designed with an aminated linker to mask strong negative

charges found in the CB portion, so the tag has an overall positive charge [19]. The Histone-Label has isoelectric points of 10.2 which means it is positively charged at biological pH and it may not be as favorable for the tags to bind, so a lower protein:tag ratio may be necessary to limit cytotoxicity.

Delivery of the Histone-Label at protein:tag ratios of 1:3 and 1:4 showed a similar fraction of dead cells to the delivery at the higher ratios (Figure 5). When imaging the cells at a higher magnification, however, a lower level of delivery of the Histone-Label can be seen in many of the living cells. The concentrations of the Histone-Label incubated for delivery at these lower ratios are comparable to the manufacturer's suggested range for immunohistochemistry (a dilution of 1:200-1:1000 or about 0.04 μM to 0.35 μM), but the fluorescence intensity shown by the live cell delivery method is much lower than that visible in fixed cell staining. This suggests that only a fraction of the tagged proteins are making it into the cytosol and reaching their targets. While raising the protein concentration would increase the number of delivered proteins, the increase of tag concentration would lead to a higher level of cytotoxicity.

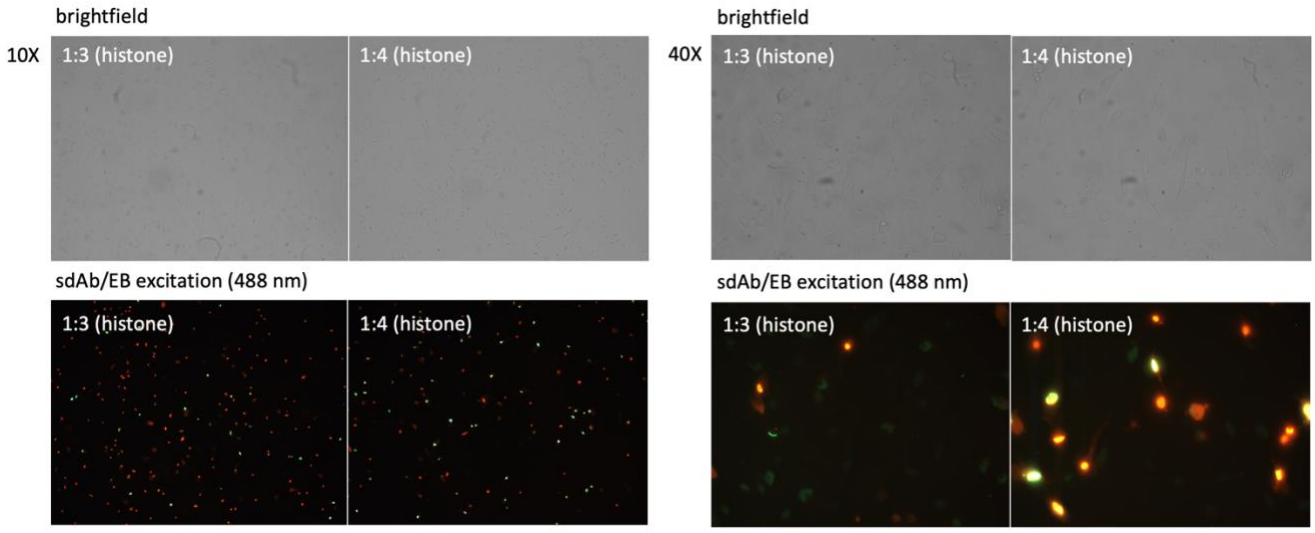

Figure 5: *Histone-Label delivered using protein:tag ratios of 1:3 and 1:4. Each condition used a final tag concentration of 2 μM. Dead cells were stained with EB according to protocol.*

While the lower concentration delivery shown by the Histone-Label is not optimal for imaging applications, it shows that there is a level of delivery that is possible without cytotoxicity in those specific cells. This could be further explored for therapeutic applications that may not need as high a concentration of delivery as is necessary for imaging applications.

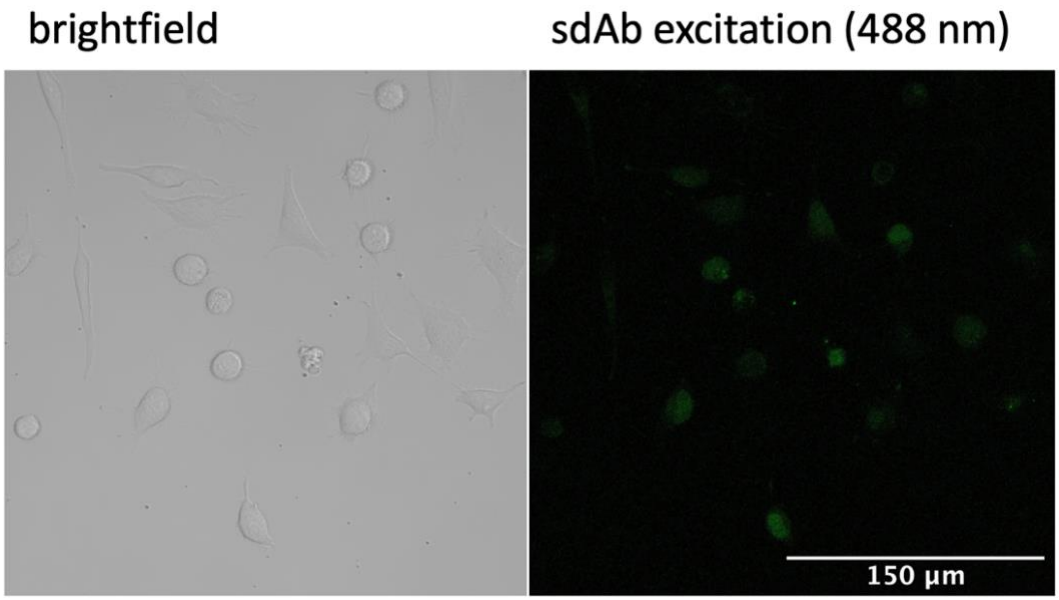

Figure 6: *Confocal images of Histone-Label delivered using a protein:tag ratio of 1:5 with a final tag concentration of 2 µM.*

Confocal imaging of the Histone-Label delivered at a protein:tag ratio of 1:5 showed the same lower concentration delivery as widefield imaging at the lower ratios (Figure 6). In comparison to the brightfield image, the faintly stained nuclei can be seen in cells that have maintained adhesion to the plate and look healthy, as well as some that have a rounder appearance and may be in the process of cell death.

Fab Fragments:

A secondary antibody-derived Fab fragment was used for testing with the alkyl-CB tag delivery method because secondary antibodies are cheaper and readily available at higher concentrations. A high concentration is necessary due to dilution during the digestion process. The Fab fragments were delivered at a protein to tag ratio of about 1:12, a ratio that was previously shown to have functionality with BSA, a similarly sized protein [19]. Delivery of the Fab fragments was not visible at 10X magnification, but images taken at 40X magnification showed successful delivery to about half the cells (Figure 7). The secondary Fab fragments are evenly distributed within the cytosol, with a few bright fluorescent spots that suggest aggregation. The even distribution within the cytosol means that the Fab fragments have not entered the cell through endocytosis, as the fluorescence is not concentrated in endosomal vesicles. The visible bright spots are suspected to be aggregates, rather than endosomal vesicles due to the visible dark spots in the bright field image, as well as their presence on the plate's surface distant from any cells. Staining of dead cells shows cell death in about a quarter of the visible cells, but the cells with the strongest visible delivery were not dead. This points to the possibility that free-floating tags may be a strong factor in cytotoxicity of the delivery method, rather than the delivery of tag-bound proteins causing cell death.

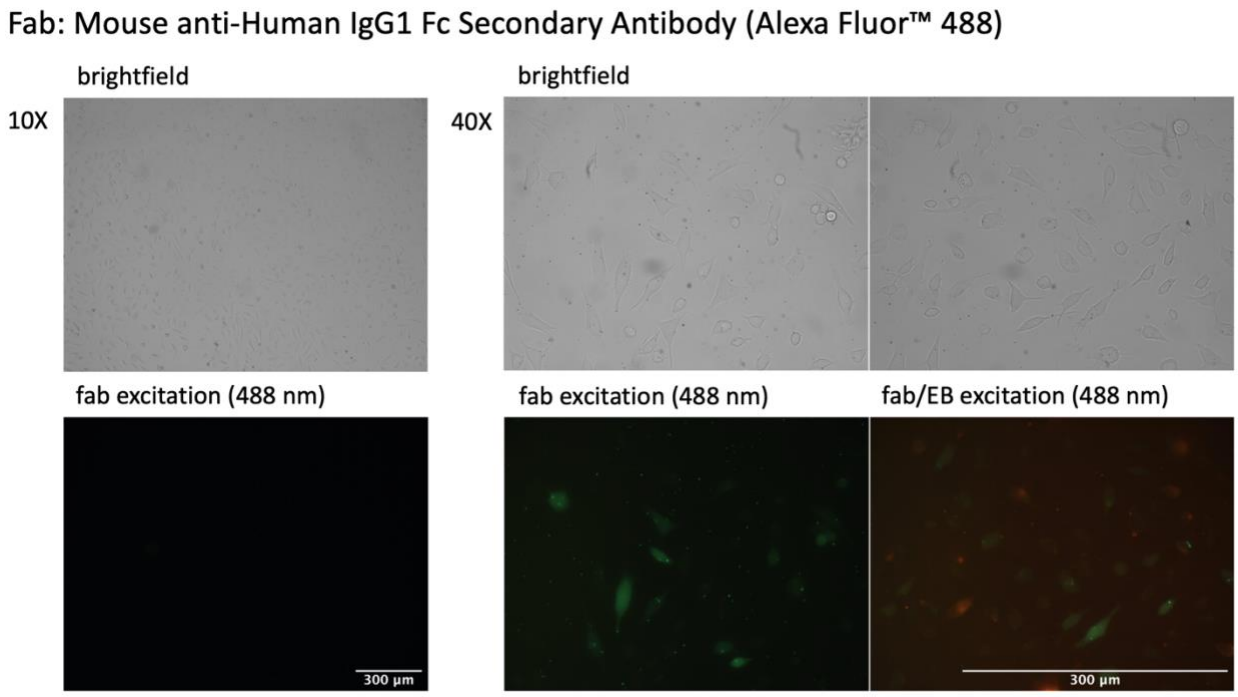

Figure 7: *Secondary Fab fragment delivered using a protein:tag ratio of 1:12 and a final tag concentration of 1 µM. Dead cells were stained with EB according to protocol. Brightfield and fluorescent images were taken at 10X and 40X magnification.*

Confocal imaging of Fab fragments delivered at a protein to tag ratio of about 1:12 showed similar results to the widefield images (Figure 8). Distributed cytosolic delivery was visible in a couple of the imaged cells, while one cell showed a higher concentration of aggregated Fab fragments. Aggregates were also visible elsewhere on the plate's surface.

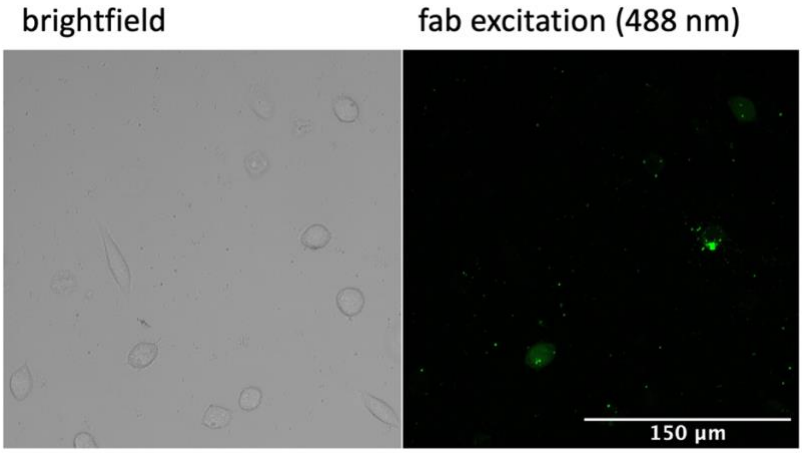

Figure 8: *Confocal images of secondary Fab fragment delivered using a protein:tag ratio of 1:12 with a final tag concentration of 1 µM.*

Full-Sized Antibodies:

Four antibodies were chosen for testing with the alkyl-CB tag delivery method. The Mouse anti-Human IgG1 Fc Secondary Antibody, Alexa Fluor™ 488 (Secondary Antibody) was chosen to allow direct comparison of delivery efficacy between Fab fragments and full-sized antibodies. Delivery of the Secondary Antibody at a protein:tag ratio of 1:16 showed successful delivery into some cells, but there were many more bright aggregate spots than was seen in the Fab delivery (Figure 9). Some of these bright spots were visible at 10X magnification, but the dispersed cytosolic fluorescence was only visible at 40X magnification. The bright spots visible at 40X magnification corresponded to dark spots visible in the brightfield image. About a third of visible cells experienced cell death when exposed to the antibody delivery method, but like with the Fab fragments, cells showing the most visible delivery of antibodies were not dead.

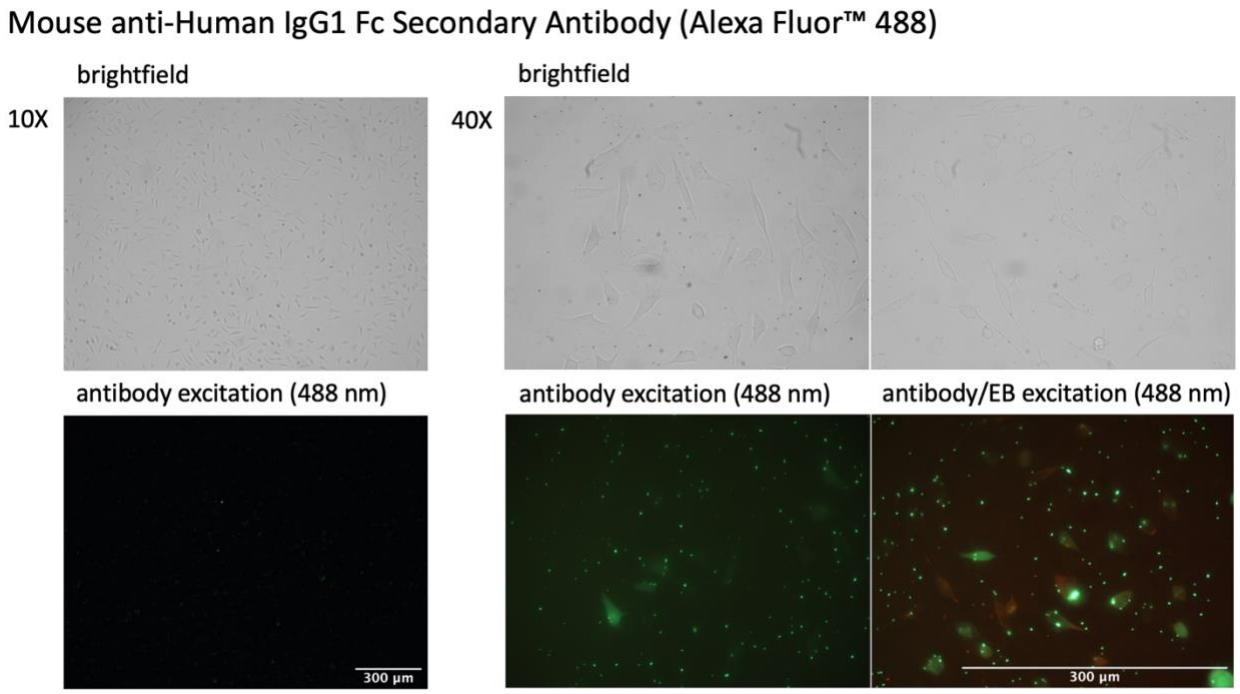

Figure 9: *Secondary antibody delivered using a protein:tag ratio of 1:16 with a final antibody concentration of 0.062 µM and a final tag concentration of 1 µM. Dead cells were stained with EB according to protocol. Brightfield and fluorescent images were taken at 10X and 40X magnification.*

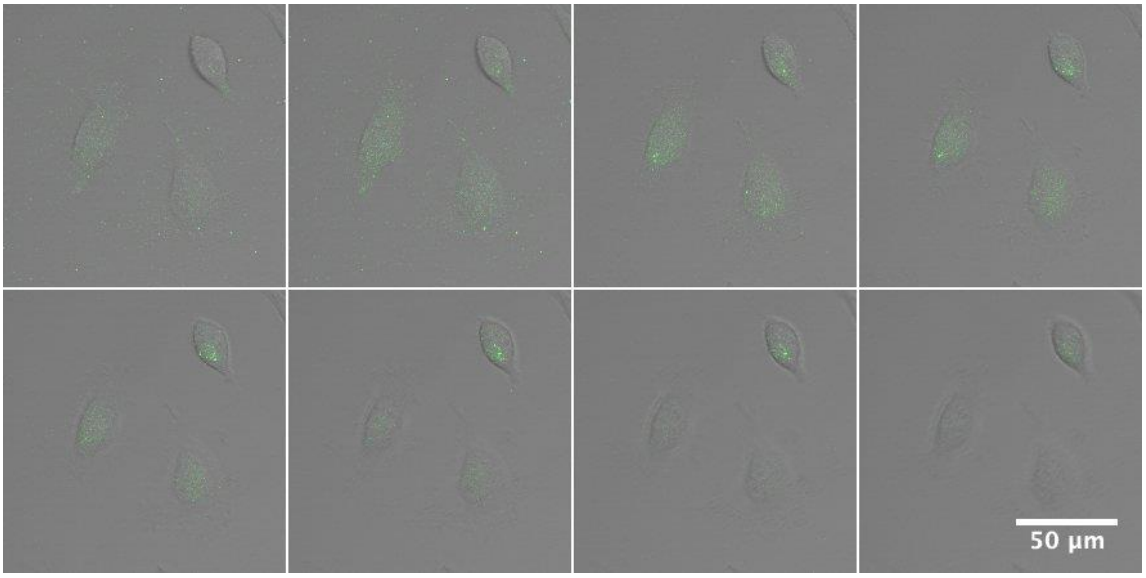

Figure 10: *Secondary antibody delivered using a protein:tag ratio of 1:16 with a final antibody concentration of 0.062 µM and a final tag concentration of 1 µM. Confocal images taken using a 20X dry objective. Images represent 8 focal slices over a depth of 7.98 µM above the plate's surface. Images are read from right to left and top to bottom moving up from the plate's surface.*

Confocal imaging was also performed on cells that underwent delivery of the Secondary Antibody at a protein:tag ratio of 1:16 to show that the antibodies were delivered within the cells, rather than adhered to the membrane. Images were taken at evenly spread focal planes within a range of 7.98 µM to include the height of the whole cell, about 5 µM [22]. Images showed fluorescence within the cells at each plane, suggesting that the antibodies have entered inside the cell (Figure 10).

The Alexa Fluor® 488 anti-Vimentin Antibody (Vimentin Antibody) was chosen to see if antibody binding capabilities are retained after delivery and if a high enough concentration could be delivered to visualize the filament structure of the vimentin target. Delivery of the Vimentin Antibody at a protein:tag ratio of 1:20 showed some successful delivery, however, most cells did not show the expected vimentin structure (Figure 9). Most cells that exhibited delivery showed a somewhat dispersed fluorescence, but it was not as uniform as that seen using the Secondary

Antibody. It is possible that the antibodies delivered within the cell were binding to the vimentin target, but there was not a high enough concentration of the antibody within the cell for binding and visualization of entire filaments. There were many bright aggregate spots, some of which were visible at 10X magnification, but the dispersed cytosolic fluorescence was only visible at 40X magnification. The dark spot aggregates visible in the 40X brightfield images were smaller than those seen in the Secondary Antibody delivery. The number of cells experiencing cell death in this experiment was only about one tenth of visible cells.

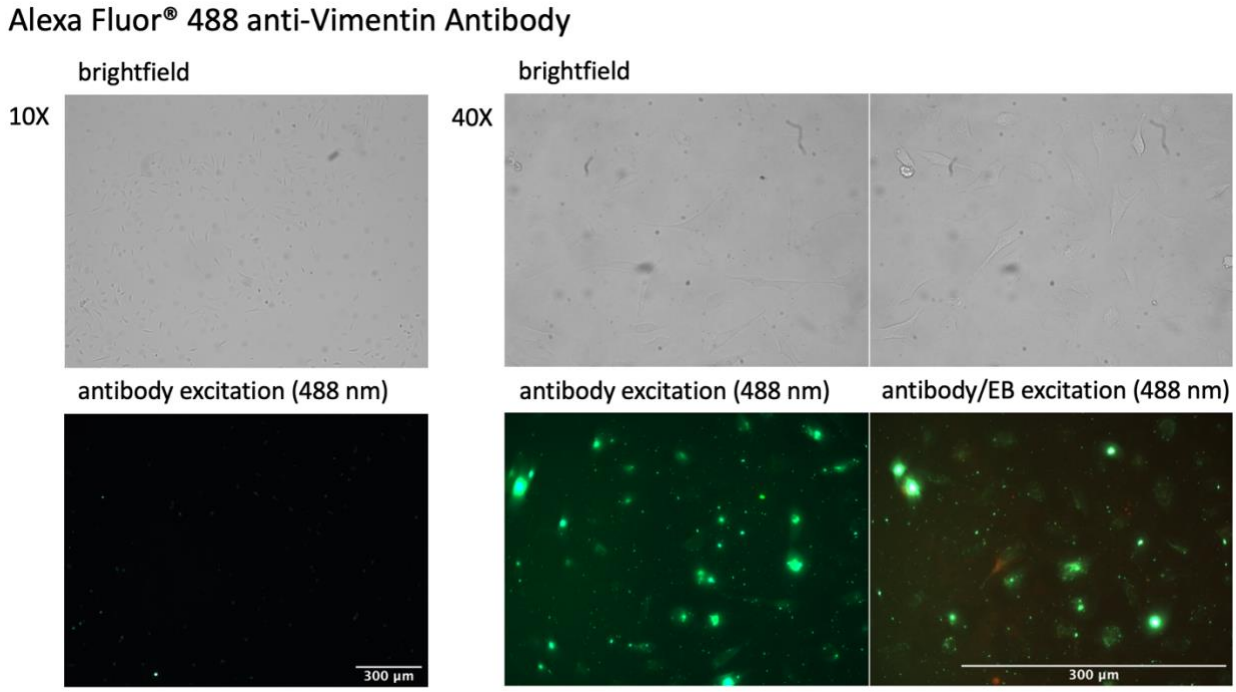

Figure 10: *Anti-vimentin antibody delivered using a protein:tag ratio of 1:20 with a final antibody concentration of 0.05 µM and a final tag concentration of 1 µM. Dead cells were stained with EB according to protocol. Brightfield and fluorescent images were taken at 10X and 40X magnification.*

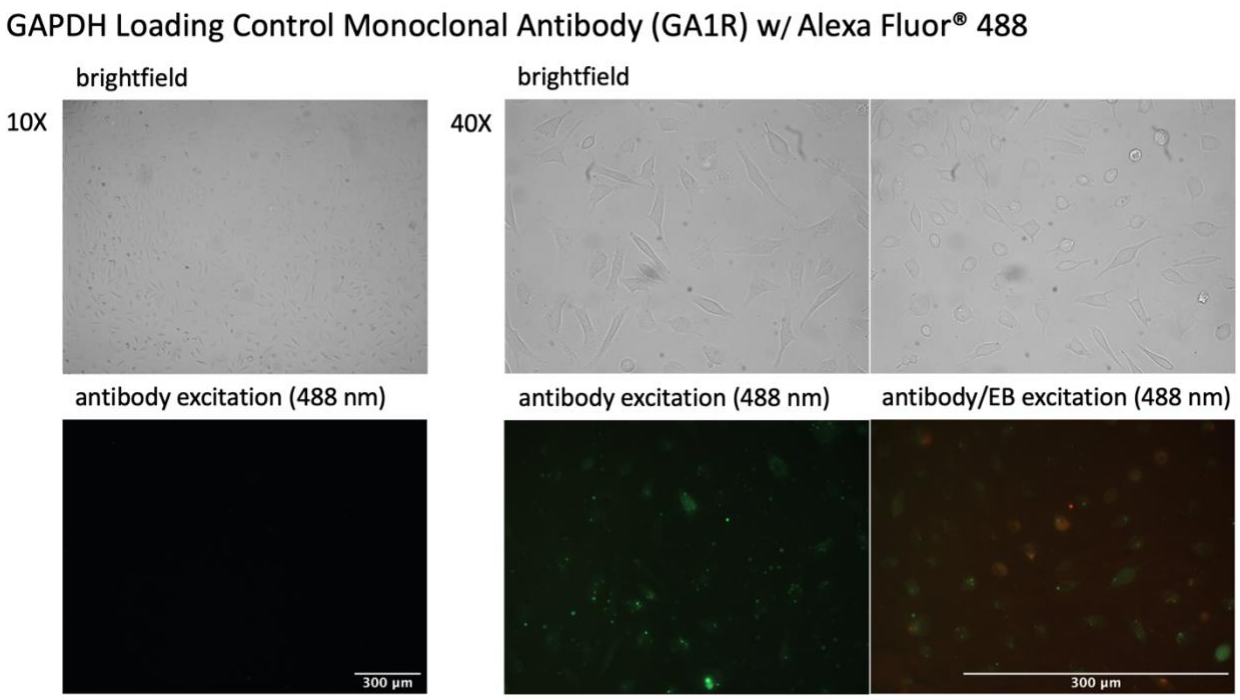

Figure 11: *Anti-GAPDH antibody delivered using a protein:tag ratio of about 1:25 with a final antibody concentration of 0.04 µM and a final tag concentration of 1 µM. Dead cells were stained with EB according to protocol. Brightfield and fluorescent images were taken at 10X and 40X magnification.*

The GAPDH Loading Control Monoclonal Antibody GA1R (GAPDH Antibody) was chosen as another dispersed cytosolic target, with expected stronger binding around the edges of the cell. Delivery of the GAPDH Antibody at a protein:tag ratio of 1:25 showed some successful delivery and dispersion within the cytosol, despite the lower protein concentration, but there was no localization at the edges as expected (Figure 11). There were fewer aggregates than seen with the other antibodies, with nothing visible at 10X magnification and minimal visualization of aggregates in the brightfield images. The lower number of aggregates may be due to the lower protein concentration overall. Cell death occurred in about half of visible cells. This higher level of cytotoxicity is most likely due to the higher protein:tag ratio and possibility of more free-floating tags.

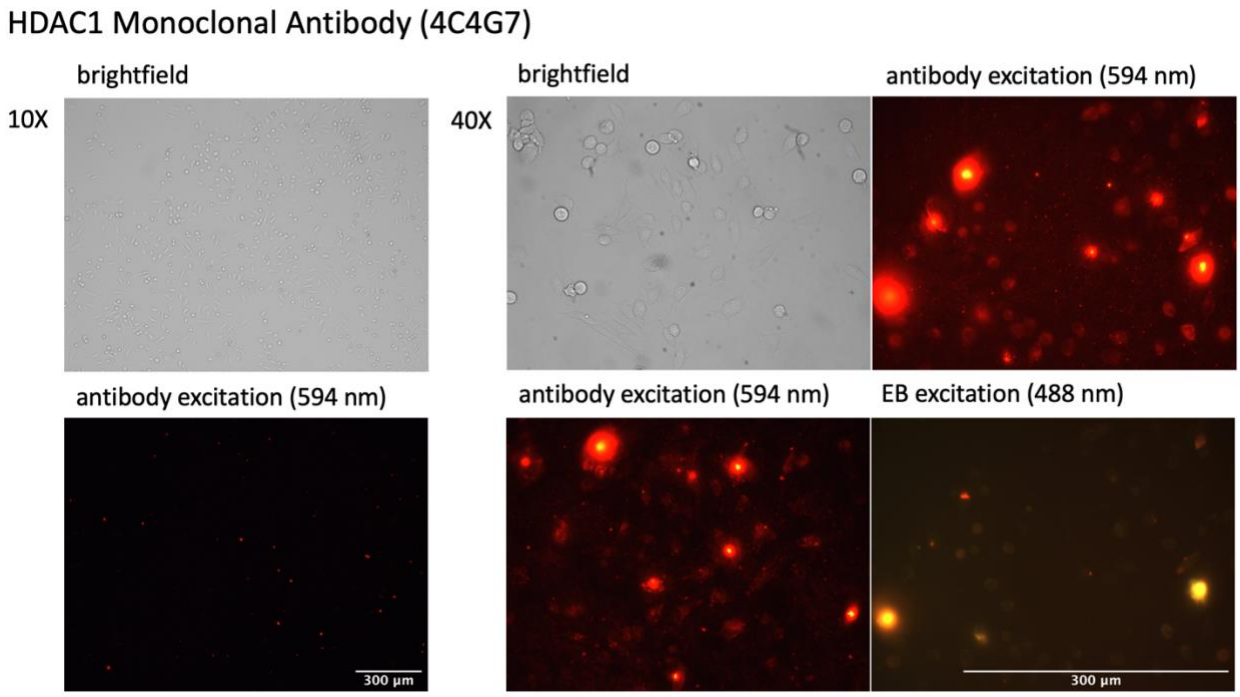

Figure 12: *Anti-HDAC1 antibody delivered using a protein:tag ratio of 1:8 with a final antibody concentration of 0.125 µM and a final tag concentration of 1 µM. Dead cells were stained with EB according to protocol. Brightfield and fluorescent images were taken at 10X and 40X magnification.*

The HDAC1 Monoclonal Antibody 4C4G7 (Histone Antibody) was chosen as a comparison against the Histone-Label in terms of target binding. Previous studies have shown that proteins larger than 60 kDa are not able to diffuse through the nuclear envelope, so it is possible that these antibodies are too large to reach their target [23]. Delivery of the Histone Antibody at a protein:tag ratio of 1:8 showed successful delivery and some dispersion within the cytosol (Figure 12). There was not localization to the nucleus, most likely due to the size of the antibodies. There were some very bright spots with high visibility at 10X magnification and 40X magnification seen in this delivery. Despite the strength of fluorescence of these spots, there were not visible aggregate spots in the bright field images. About half the cells showing visible delivery by fluorescence also showed cell death.

One drawback to the intracellular delivery method is the amount of antibody solution necessary for successful visualization. The suggested dilution levels for fixed delivery of each of these antibodies range from 1:20 to 1:1000 putting the suggested final concentration in the nanomolar range. The final concentrations for all the antibodies undergoing alkyl-CB tag delivery were in the micromolar range, meaning at least a ten-fold increase in the amount of antibody is necessary to reach the somewhat similar visualization results.

One variable that may contribute to efficacy in delivery of antibodies is the antibody's isoelectric point. As stated, regarding sdAbs, proteins with isoelectric points above biological pH (about 7.4) may have a lower affinity for binding of the alkyl-CB tag. Most antibodies, including those used in this paper, do not have isoelectric points that are tested or provided by the manufacturers, however, testing of 25 clinically approved antibodies showed their isoelectric points ranging from 6.1 to 9.2 [24]. With no common isoelectric point for antibodies and, therefore, Fab fragments, this may be an important area to investigate in future studies. Especially because tag-protein binding affinity and the presence of loose tags in the incubation solution seem to influence cytotoxicity of the delivery method.

CONCLUSION:

While this study showed some level of success in sdAb delivery into live cells, further testing is necessary to fully understand the efficacy of this tagging delivery method on more positively charged proteins such as sdAbs. The current protocol results in a low concentration of delivered proteins and a moderate level of cytotoxicity, so in further studies the goal would be to increase

delivered concentration and decrease the cytotoxicity. One solution that may minimize cytotoxicity of the method could be adjustment of the linker used in the tag to increase the negative charge, so the binding between tag and protein is stronger. Another option to increase efficacy could be reversible modification of the charges on the sdAbs to strengthen tag binding, a method that has been used previously for intracellular delivery [25]. Success with either of these options could lead to fewer free-floating tags in the solution and minimize cell membrane disruption.

The most promising object of delivery tested in this paper was the Fab fragment. There was a workable concentration of the protein delivered into a fraction of the cells and, while there was cytotoxicity, the cells that showed delivery were not the ones experiencing cell death. Further testing with of Fab fragments that bind to intracellular targets could help us learn if the delivered concentration is high enough to allow visualization of target structures, such as vimentin, as well as if the Fab fragments can enter the nuclear envelope.

All four of the antibodies tested showed some level of successful delivery, but visualization of targets to show their intracellular structures was generally not successful. In the cases of the Vimentin Antibody and GAPDH Antibody, this lack of visualization was most likely due to the lower concentration of antibodies available in the cell for target binding. For the Histone Antibody, however, it is possible that reaching targets in the nucleus is not possible for proteins at 150 kDa. Due to the cost of purchasing high concentrations of primary antibodies, an important aspect of future studies would be to decrease the concentration of antibodies necessary for delivery. This would increase the feasibility of use of the delivery method for more

researchers. One option to decrease the necessary concentration could be adjustments to the tag to increase binding affinity, such as those described when discussing sdAb efficiency. Ensuring that all proteins have the number of bound tags necessary to enter the cell should increase the amount that experience a successful delivery process. Another option could be adjustments to the protocol for delivery such as minimizing the level of solution necessary during incubation.

While future studies probing the efficacy of this method are necessary before it would be ready for widespread use, the alkyl-CB tag delivery method shows promise for use in the fields of cell therapy and imaging.

ACKNOWLEDGEMENTS:

Thanks to Xiaohu Gao for mentorship and guidance in completion of this project and participation as a committee member. Thanks to Dr. Andre Berndt for participation in my committee. Thanks to Samuel Jeong for synthesis of the alkyl-CB tag, as well as support and collaboration in the lab. Thanks to Wanyi Tai and Pengfei Zhao for their preliminary work on the cholesterol- and hydrophobic-tag delivery method. I wish to acknowledge my use of the confocal microscope at the W. M. Keck Microscopy Center and the help of the Keck Center Manager, Dr. Nathaniel Peters. I also wish to acknowledge the scholarship support provided by the Mary Gates Endowment for this research.

REFERENCES:

[1] A. P. Russ and S. Lampel, "The druggable genome: an update," *Drug Discovery Today*, vol. 10, no. 23, pp. 1607–1610, Dec. 2005, doi: 10.1016/S1359-6446(05)03666-4.

[2] G. Zhang, J. Zhang, Y. Gao, Y. Li, and Y. Li, "Strategies for targeting undruggable targets," *Expert Opinion on Drug Discovery*, vol. 17, no. 1, pp. 55–69, Jan. 2022, doi: 10.1080/17460441.2021.1969359.

[3] I. A. Prior, P. D. Lewis, and C. Mattos, "A comprehensive survey of Ras mutations in cancer," *Cancer Res*, vol. 72, no. 10, pp. 2457–2467, May 2012, doi: 10.1158/0008-5472.CAN-11-2612.

[4] X. Huang and V. M. Dixit, "Drugging the undruggables: exploring the ubiquitin system for drug development," *Cell Res*, vol. 26, no. 4, Art. no. 4, Apr. 2016, doi: 10.1038/cr.2016.31.

[5] J. S. Lazo and E. R. Sharlow, "Drugging Undruggable Molecular Cancer Targets," *Annu. Rev. Pharmacol. Toxicol.*, vol. 56, no. 1, pp. 23–40, Jan. 2016, doi: 10.1146/annurev-pharmtox-010715-103440.

[6] T. A. Slastnikova, A. V. Ulasov, A. A. Rosenkranz, and A. S. Sobolev, "Targeted Intracellular Delivery of Antibodies: The State of the Art," *Front. Pharmacol.*, vol. 9, 2018, doi: 10.3389/fphar.2018.01208.

[7] S. Niamsuphap, C. Fercher, S. Kumble, P. Huda, S. M. Mahler, and C. B. Howard, "Targeting the undruggable: emerging technologies in antibody delivery against intracellular targets," *Expert Opinion on Drug Delivery*, vol. 17, no. 9, pp. 1189–1211, Sep. 2020, doi: 10.1080/17425247.2020.1781088.

[8] D. J. Stephens and V. J. Allan, "Light Microscopy Techniques for Live Cell Imaging," *Science*, vol. 300, no. 5616, pp. 82–86, Apr. 2003, doi: 10.1126/science.1082160.

[9] J. Lippincott-Schwartz and G. H. Patterson, "Development and Use of Fluorescent Protein Markers in Living Cells," *Science*, vol. 300, no. 5616, pp. 87–91, Apr. 2003, doi: 10.1126/science.1082520.

[10] K. Im, S. Mareninov, M. F. P. Diaz, and W. H. Yong, "An introduction to Performing Immunofluorescence Staining," *Methods Mol Biol*, vol. 1897, pp. 299–311, 2019, doi: 10.1007/978-1-4939-8935-5_26.

[11] J. M. Warram *et al.*, "Antibody Based Imaging Strategies of Cancer," *Cancer Metastasis Rev*, vol. 33, no. 0, pp. 809–822, Sep. 2014, doi: 10.1007/s10555-014-9505-5.

[12] R. Atreya *et al.*, "In vivo imaging using fluorescent antibodies to tumor necrosis factor predicts therapeutic response in Crohn's disease," *Nat Med*, vol. 20, no. 3, pp. 313–318, Mar. 2014, doi: 10.1038/nm.3462.

[13] A. Fu, R. Tang, J. Hardie, M. E. Farkas, and V. M. Rotello, "Promises and Pitfalls of Intracellular Delivery of Proteins," *Bioconjug Chem*, vol. 25, no. 9, pp. 1602–1608, Sep. 2014, doi: 10.1021/bc500320j.

[14] S. Kumari, S. Mg, and S. Mayor, "Endocytosis unplugged: multiple ways to enter the cell," *Cell Research*, vol. 20, no. 3, Art. no. 3, Mar. 2010, doi: 10.1038/cr.2010.19.

[15] R. F. Gahl, "Microinjection of Live Mammalian Cells: A Delivery Method that Provides Added Versatility to the Study of Cellular Function," in *Microinjection: Methods and Protocols*, C. Liu and Y. Du, Eds. New York, NY: Springer, 2019, pp. 525–536. doi: 10.1007/978-1-4939-8831-0_30.

[16] M. L. Yarmush, A. Golberg, G. Serša, T. Kotnik, and D. Miklavčič, “Electroporation-based technologies for medicine: principles, applications, and challenges,” *Annu Rev Biomed Eng*, vol. 16, pp. 295–320, Jul. 2014, doi: 10.1146/annurev-bioeng-071813-104622.

[17] B. Chatin *et al.*, “Liposome-based Formulation for Intracellular Delivery of Functional Proteins,” *Molecular Therapy - Nucleic Acids*, vol. 4, p. e244, Jan. 2015, doi: 10.1038/mtna.2015.17.

[18] H. Chang *et al.*, “Rational Design of a Polymer with Robust Efficacy for Intracellular Protein and Peptide Delivery,” *Nano Lett.*, vol. 17, no. 3, pp. 1678–1684, Mar. 2017, doi: 10.1021/acs.nanolett.6b04955.

[19] W. Tai, P. Zhao, and X. Gao, “Cytosolic delivery of proteins by cholesterol tagging,” *Sci Adv*, vol. 6, no. 25, p. eabb0310, Jun. 2020, doi: 10.1126/sciadv.abb0310.

[20] P. Holliger and P. J. Hudson, “Engineered antibody fragments and the rise of single domains,” *Nat Biotechnol*, vol. 23, no. 9, Art. no. 9, Sep. 2005, doi: 10.1038/nbt1142.

[21] G. Gonzalez-Sapienza, M. A. Rossotti, and S. Tabares-da Rosa, “Single-Domain Antibodies As Versatile Affinity Reagents for Analytical and Diagnostic Applications,” *Front. Immunol.*, vol. 8, 2017, doi: 10.3389/fimmu.2017.00977.

[22] A. Gigler, M. Holzwarth, and O. Marti, “Local nanomechanical properties of HeLa-cell surfaces,” *J. Phys.: Conf. Ser.*, vol. 61, pp. 780–784, Apr. 2007, doi: 10.1088/1742-6596/61/1/156.

[23] B. Alberts, A. Johnson, J. Lewis, M. Raff, K. Roberts, and P. Walter, “The Transport of Molecules between the Nucleus and the Cytosol,” *Molecular Biology of the Cell. 4th edition*, 2002, Accessed: May 18, 2022. [Online]. Available: http://www.ncbi.nlm.nih.gov/books/NBK26932/

[24] A. Goyon *et al.*, “Determination of isoelectric points and relative charge variants of 23 therapeutic monoclonal antibodies,” *Journal of Chromatography B*, vol. 1065–1066, pp. 119–128, Oct. 2017, doi: 10.1016/j.jchromb.2017.09.033.

[25] M. Wang, K. Alberti, S. Sun, C. L. Arellano, and Q. Xu, “Combinatorially designed lipid-like nanoparticles for intracellular delivery of cytotoxic protein for cancer therapy,” *Angew Chem Int Ed Engl*, vol. 53, no. 11, pp. 2893–2898, Mar. 2014, doi: 10.1002/anie.201311245.

APPENDIX A: Tag Synthesis

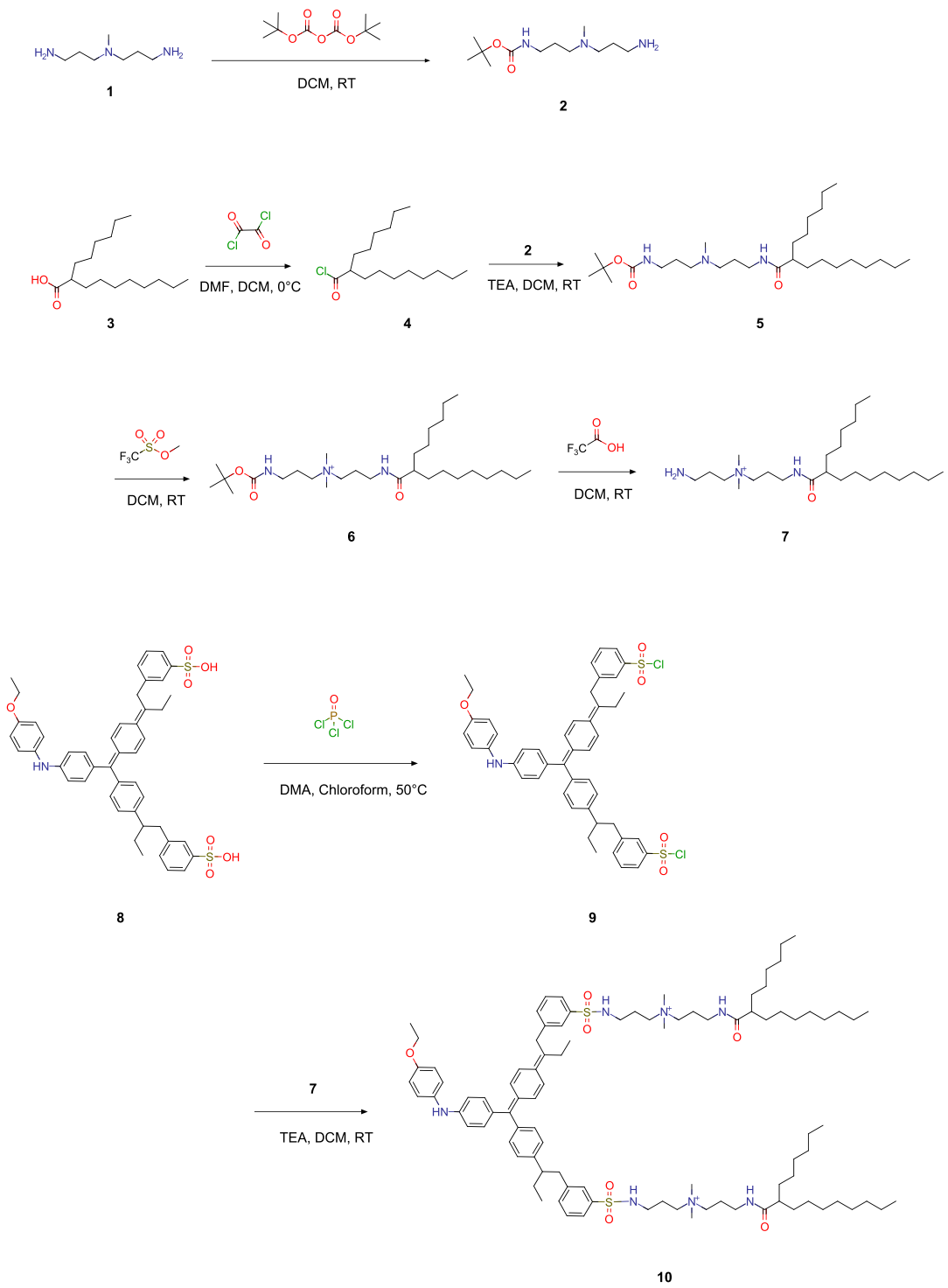

Scheme 1: *Synthetic route of the CB-alkyl tag (**10**). Hexyl decanoyl chloride (**4**) was reacted with the linker **2** to obtain compound **5**, whose tertiary amine is subsequently methylated to the quaternary amine (**6**). After t-Boc deprotection, two copies of **7** were conjugated to Coomassie blue G250, resulting in the final product, CB-alkyl tag (**10**).*

The CB-alkyl tag (compound **10**) was synthesized according to the previous report (W. Tai, P. Zhao, X. Gao, *Sci. Adv.* 2020; **6**:eabb0310) with modifications.

(a) Tert-butyl N-{3-[(3-aminopropyl)(methyl)amino]propyl}carbamate (2)

Bis(3-aminopropyl)(methyl)amine (**1**) (72.6 g, 500 mmol) was dissolved in 500 ml of dry dichloromethane (DCM). The reaction was cooled to 0 °C, and di-tert-butyl decarbonate (11.5 ml, 50 mmol) was slowly added dropwise over 24 hours. After addition was complete, the reaction mixture was allowed to warm up to RT and stirred for 12 hours. To remove access compound **1**, the reaction mixture was washed five times with water. The organic phase was dried with anhydrous Na_2SO_4 and concentrated in vacuo. The product **2** was used in the next step without further purification.

(b) 2-hexyldecanoyl chloride (4)

2-hexyldecanoic acid (**3**) (3.0 g, 11.7 mmol) was dissolved in dry DCM (50 ml), and cooled down in an ice bath. Oxalyl chloride (1.09 ml, 12.9 mmol) was slowly added dropwise. 5 drops of DMF was added as catalyst. Reaction was proceeded until the bubbling is ceased. Reaction mixture was concentrated in vacuo, providing yellowish oil. The crude product **4** was used in the next step without further purification.

(c) tert-butyl N-(3-{[3-(2-hexyldecanamido)propyl](methyl)amino}propyl)carbamate (5)

Compound **2** (3.17 g, 12.9 mmol) was dissolved in dry DCM (30 ml), stirred, and cooled down in an ice bath. To this solution, 20 ml of dry DCM solution of 2-hexyldecanoyl chloride (4) (3.22

g, 11.7 mmol) was added, followed by triethylamine (1.8 ml, 12.9 mmol). The reaction mixture was allowed to warm up to RT and stirred overnight. The reaction mixture was washed with water three times, and the organic phase was separated, dried with anhydrous Na_2SO_4 and concentrated in vacuo. The crude product was loaded onto silica gel and purified by flash column chromatography (DCM, and then, 10% MeOH in DCM) yielding the compound **5** (5.61g, 99.11% yield).

(d) tert-butyl N-(3-{[3-(2-hexyldecanamido)propyl]dimethylazaniumyl}propyl)carbamate (6)

Compound **5** (5.61 g, 11.596 mmol) was dissolved in anhydrous DCM (100 ml) under N_2 atmosphere. The solution was stirred and cooled to 0 °C in an ice bath. MeOTf (2.54 mL, 23.19 mmol) was slowly added dropwise to the solution. After addition was complete, the reaction mixture was allowed to warm up to RT and stirred for 12 hours. The reaction was cooled to 0 °C in an ice bath, and then 30ml of deionized water was slowly added to the reaction mixture to quench excess MeOTf. After stirring 1 hour, solvent was evaporated under reduced pressure. The crude product **6** was used in the next step without further purification.

(e) (3-aminopropyl)[3-(2-hexyldecanamido)propyl]dimethylazanium (7)

Compound **6** (5.74 g, 11.5 mmol) was dissolved in dry DCM (100 ml). The solution was stirred and cooled to 0 °C in an ice bath. TFA (5 ml, 65.8 mmol) was slowly added to the solution. reaction mixture was allowed to warm up to RT and stirred overnight. The reaction mixture was concentrated in vacuo. The crude product **7** was used in the next step without further purification.

(f) CB-alkyl tag (10)

Coomassie blue G-250 (**8**) (100 mg, 0.117 mmol) was dissolved in anhydrous DMA (10 ml) and chloroform (15 ml) under N_2 atmosphere. To the solution, phosphorus(V) oxychloride (100 µL, 1.05 mmol) was slowly added dropwise. The reaction mixture was refluxed for 2 hours at 50 °C and then cooled to RT. Chilled dry ethyl ether (100 ml) was added to the reaction mixture to precipitate the product. The precipitated compound **9** was filtered, washed with ether, dried in vacuo, and resuspended in 10 ml of anhydrous DCM. To the solution, 10 ml of dry DCM solution of compound **7** was added, followed by triethylamine (100 µl). The reaction mixture was stirred at RT overnight. The reaction mixture was washed with water three times, and the organic phase was separated, dried with anhydrous Na_2SO_4, and concentrated in vacuo. The crude product was loaded onto silica gel and purified by flash column chromatography (90:10:1 DCM:MeOH:NH_4OH) yielding the compound **10**.